PCCP

Accepted Manuscript

This is an *Accepted Manuscript*, which has been through the Royal Society of Chemistry peer review process and has been accepted for publication.

Accepted Manuscripts are published online shortly after acceptance, before technical editing, formatting and proof reading. Using this free service, authors can make their results available to the community, in citable form, before we publish the edited article. We will replace this *Accepted Manuscript* with the edited and formatted *Advance Article* as soon as it is available.

You can find more information about *Accepted Manuscripts* in the Information for Authors.

Please note that technical editing may introduce minor changes to the text and/or graphics, which may alter content. The journal's standard Terms & Conditions and the Ethical guidelines still apply. In no event shall the Royal Society of Chemistry be held responsible for any errors or omissions in this *Accepted Manuscript* or any consequences arising from the use of any information it contains.

ROYAL SOCIETY OF CHEMISTRY

www.rsc.org/pccp

Novel pnicogen bonding interactions with silylene as an electron donor: Covalency, unusual substituent effects and new mechanisms

Hongying Zhuo, Qingzhong Li*

The Laboratory of Theoretical and Computational Chemistry, School of Chemistry and Chemical Engineering, Yantai University, Yantai 264005, People's Republic of China

Corresponding author:

Qingzhong Li Dr

The Laboratory of Theoretical and Computational Chemistry

School of Chemistry and Chemical Engineering

Yantai University

Yantai 264005

People's Republic of China

Tel. (+086) 535 6902063

Fax. (+086) 535 6902063

E-mail: lqz@ytu.edu.cn

Abstract

An analogue of carbene, singlet silylene $(H_3P{=}N)_2Si$ was paired with the mono-substitution phosphines XH_2Y (X = P, As, and Sb; Y = F, Cl, Br, and I) to form unconventional pnicogen-bonded complexes. All structures have C_s symmetry except the Sb complex, showing a deviation from this symmetry due to the coexistence of H···H interaction. The P and As complexes have different geometries from conventional pnicogen-bonded ones because the Y−X···Si line has a big deviation from the molecular plane composed of two N atoms and one Si atom of $(H_3P{=}N)_2Si$. This deviation can be attributed to a new formation mechanism of pnicogen bond with a combinative result of the $LP_{Si}\rightarrow BD^*_{X\text{-}Y}$ and $LP_X\rightarrow LP^*_{Si}$ orbital interactions. Generally, the pnicogen bond becomes stronger in the order of F < Cl < Br < I and weaker in the order of P > As > Sb, exhibiting an unexpected substitution effect and dependence on the nature of pnicogen atom. These orders are inconsistent with the MEP on the X atom but can be better explained with the above orbital interactions. The Si···X interaction displays a character of covalent or partially covalent interaction, evidenced by the big interaction energy of -59.9 ~ -105.4 kJ/mol as well as the negative energy density and the great charge transfer.

Keywords: Silylene; Pnicogen bond; Orbital interactions

1. Introduction

Since pnicogen bonding was proposed as a new molecular linker in crystal materials by Hey-Hawkins *et al*,[1] theoretical investigations on pnicogen bonds have greatly increased, particularly for P···P and P···N interactions.[2-16] Of course, experimental studies with such interactions have been performed for many years, which has been pointed out by Politzer *et al*[17] and surveyed in the Cambridge Crystallographic Database.[18] Among all the reported pnicogen bonds, the most discussed one is P···N pnicogen bond, with the lone pair on the N atom of NH_3 directly interacting with the sp^3 hybridized P atom.[5,7,9-16] For $H_3P\cdots NH_3$ heterodimer, one of the three H atoms in both molecules locates almost oppositely along the P···N axis, with an interaction energy of -8.6 kJ/mol.[13] As this H atom in H_3P is replaced by an electron-withdrawing group, the P···N distance is decreased, accompanied with the increase of interaction energy, whereas the electron-donating methyl group slightly weakens this interaction.[19] However, the di- and tri-halogenated PH_3 causes the P···N interaction weakened with respect to the mono-halogenated one,[20] being reverse to that in hydrogen bonds, where each additional halogen atom progressively strengthens the interaction.[21]

Actually, the interactions between positive σ-holes on Group V atoms and negative sites were shown earlier by Murray and Politzer with computational methods.[22-24] Molecular electrostatic potential (MEP) analysis shows that there is a region of positive MEP (σ-hole) near the P atom, thus the electrostatic interaction between the positively charged σ–hole on the sp^3 hybridized pnicogen atom and the

electron donor is responsible for the stability of pnicogen-bonded complexes.[19] On the other hand, Scheiner ascribed its origin to the charge transfer from the N lone pair into the σ* antibonding orbital of a P–X bond.[13] Based on the electrostatic model of pnicogen bond, it is expected that the heavier pnicogen atoms such as As and Sb would form a stronger pnicogen bond.[25] In addition, NO_2X (X = F, Cl, CN, and NO_2)[26] and PO_2X (X = F, Cl, and Br)[27] can provide a π-hole to participate in pnicogen bonds. In the above pnicogen bonds, the electron donors are the lone pairs from PH_3, H_2CO, H_2CS, H_2O, and H_2S.[28] Actually, other types of electron donors including π-electrons, [25, 29-31] metal hydrides,[32] radicals,[33] and anions[34] have also been used in pnicogen bonds. However, to our knowledge, little study is performed for pnicogen bonds involving carbenes.

Carbene is a highly reactive species with short lifetime and it has been demonstrated that carbene can act as the electron donor in hydrogen bonds,[35,36] halogen bonds[37-39] lithium bonds,[40] and chalcogen bonds.[41] Due to the presence of the lone pair, singlet carbene has often been used in studying the above noncovalent interactions. Silylene is considered to be a heavier analogue of carbene, thus in this paper, we are interested in the pnicogen bonds with silylene as the electron donor. To confirm its existence with experimental methods in the future, we selected a stable singlet silylene, $(H_3P{=}N)_2Si$, to interact with mono-substituted phosphines XH_2Y (X = P, As, and Sb; Y = F, Cl, Br, and I). DFT calculations have shown that the derivatives of $(H_3P{=}N)_2Si$ are powerful neutral superbases in the gas phase and in the solvent phase,[42] thus we expect that a strong pnicogen bond would be formed with

$(H_3P{=}N)_2Si$. Then the big strength would bring out a prominent change in geometry and nature. Its mechanism has been unveiled by means of MEP and orbital interactions.

2. Computational methods

The geometries of **1**···XH_2Y (**1** is $(H_3P{=}N)_2Si$) complexes were optimized at the MP2 level of theory with the basis set aug-cc-pVTZ for all atoms except Sb and I. For both atoms, the basis set aug-cc-pVTZ-PP was adopted to account for relativistic effects. The frequency calculations were also carried out to verify that the optimized structures correspond to the stationary points on potential energy surfaces. No imaginary frequencies were found for all complexes. Interaction energy was corrected for the basis set superposition error (BSSE) with the counterpoise method by Boys and Bernardi[43] and deformation energy (DE). All calculations were performed with the use of the Gaussian 09 set of codes.[44]

Molecular electrostatic potentials (MEPs) at the 0.001 electrons $Bohr^3$ isodensity surfaces were calculated with the Wave Function Analysis-Surface Analysis Suite (WFA-SAS) program[45] at the MP2/aug-cc-pVTZ level. Natural bond orbital (NBO) analyses were performed at the HF/aug-cc-pVTZ level with the NBO 3.1 version[46] implemented in Gaussian 09 to obtain the charge on atoms and the occupancies in orbitals. The wavefunctions at the MP2/aug-cc-pVTZ level were used to obtain topological properties, electron localization function (ELF), and electron density difference (EDD) maps. Atoms in molecules (AIM) analyses were performed with AIM2000 program.[47] The maps of ELF and EDD were plotted with Multiwfn 3.01

suite of program.[48] The interaction energy was decomposed at the GGA:BLYP/TZP (small core) level using ADF2008.1 program.[49]

3. Results and discussion

3.1. Structure characteristics

It has been demonstrated that MEP maps are very useful for predicting the possible interaction sites between two molecules.[50] Thus the MEP maps of singlet silylene $(H_3P{=}N)_2Si$ (**1**) and XH_2Y (X = P, As, Sb, Y = F, Cl, Br, I) are plotted in Fig. 1 to determine the interaction mode of **1** with XH_2Y. Clearly, there is a region of negative MEP (blue) on the X atomic surface, corresponding to the lone pair on the X atom of XH_2Y. Meanwhile, an area of positive MEP (red, σ-hole) is observed at the outer side of the X atom along the X−Y bond. As a result, the X atom of XH_2Y plays a dual role of Lewis acid and base simultaneously, which has been evidenced in homotrimers $(PH_3)_3$[51] and $(PH_2X)_3$ with X = F, Cl, OH, NC, CN, CH_3, H, and BH_2[52] as well as heterotrimers LA···FH_2P···FH_2N and LA···H_3P···NH_3 (LA = BH_3, NCH, ClH, FH, FCl, and HLi).[53] The lone pair on the Si atom of **1** is characterized by the blue region near the Si atom in Fig. 1 and its shape can be clearly seen in the isosurface map of ELF (Fig. 1).

Initially, we tried to pair the σ-hole of mono-halogen substituted XH_2Y with the lone pair on the Si atom of **1**. The corresponding optimized structures are illustrated in Fig. 2. It is found that both **1**···PH_2Y and **1**···AsH_2Y have a similar structure of *Cs* symmetry along the Si···X−Y axis with the two H atoms of XH_2Y located at the two sides of this axis, while **1**···SbH_2Y structure deviates from such symmetry with one H

atom of SbH_2Y close to one H atom of PH_3 in **1**. This means that there is a weak attractive interaction between both types of H atoms in **1**···SbH_2Y. To validate this deduction, we calculated the electrostatic charge (MK) on both types of H atoms. It is found that the MK charge on the H atom of SbH_2Y is negative but that on the H atom of PH_3 in **1** is positive. This is due to the fact that Sb shows a smaller electronegativity than H, while the electronegativity of P is larger than that of H. Accordingly, the negatively charged H atom of SbH_2Y can be close to the positively charged H atom of PH_3 in **1**···SbH_2Y. The H···H contact in **1**···SbH_2Y can also be confirmed by the H···H distance (Table 1), which is close to the sum of the van der Waals radii of two H atoms in **1**···SbH_2Y. However, such H···H distances are much large in **1**···PH_2Y and **1**···AsH_2Y. In addition, the symmetry of **1**···XH_2Y can also be estimated with the H···H distances. In **1**···XH_2Y (X = P and As) complexes, two H···H distances almost equal, while both distances are clearly different in the Sb complexes.

Fig. 3 is the side view of **1**···XH_2Y in Fig. 2. Obviously, the line of Y−X···Si has a deviation from the molecular plane composed of two N atoms and one Si atom. According to the MEP and ELF maps of **1**, it is deduced that the σ-hole on the X atom of XH_2Y is inclined to interact with **1** along the direction of the lone pair on the Si atom. How to deal with this contradiction? We fall back on the orbital interactions between both molecules based on the conclusion that a primary source of pnicogen bond has been identified as charge transfer from the N lone pair to the σ* anti-bonding orbital of a P−Y bond.[19] It is expected that there is an orbital interaction of $LP_{Si}\rightarrow BD^*_{X\text{-}Y}$ in **1**···XH_2Y, where LP_{Si} is the lone pair orbital of Si and $BD^*_{X\text{-}Y}$

denotes the σ* antibonding orbital of X−Y bond. On the other hand, we think that another orbital interaction of $LP_X \rightarrow LP^*_{Si}$ is also present in **1**···XH_2Y according to the presence of the lone pair on the X atom and the unoccupied *p* orbital on the Si atom. The sketch of both types of orbital interactions in **1**···XH_2Y is plotted in Fig. 4. Both types of orbital interactions, particularly the latter one, are jointly responsible for the structural deviation of **1**···XH_2Y. With the increase of the X atomic mass, the negative MEP on the X atom is reduced in magnitude and even becomes positive in SbH_2Y (Table 2). Correspondingly, the $LP_X \rightarrow LP^*_{Si}$ orbital interaction is weaker in the order of X = P > As > Sb. This conclusion is also confirmed by the changes in the orbital occupancies of the $LP_X \rightarrow LP^*_{Si}$ orbital interaction discussed in the section 3.2. As a result, the biggest deviation in **1**···PH_2Y is attributed to the strongest $LP_P \rightarrow LP^*_{Si}$ orbital interaction, while the structure of **1**···SbH_2Y is similar to that in conventional pnicogen bonds.[13]

The distances of Si···P, Si···As, and Si···Sb are 2.356-2.439 Å, 2.516-2.661 Å, and 2.827-2.902 Å, respectively. All of them are smaller than the sum of the van der Waals radii of the respective atoms (4.51 Å for Si and P, 4.65 Å for Si and As, 4.81 Å for Si and Sb).[54] For the complexes with the same X atom, the Si···X distance is shorter with the increase of the Y atomic mass, indicative of a stronger Si···X interaction. As expected, the Si···X distance is longer with the increase of the X atomic mass. However, this change is not used to estimate the change of Si···X interaction strength due to the different X nature. In a previous study, Lommerse et al[55] suggested a ratio of $\lambda = R_{Si\cdots X}/(r_{Si}+r_X)$ to measure the interaction strength, where r_{Si} and r_X are the van

der Waals radii of Si and X atoms, respectively. This ratio is less than 1 in **1**···XH_2Y, confirming the presence of Si···X interaction. Furthermore, the smaller λ corresponds to the stronger Si···X interaction. When X is fixed and Y is varied, this ratio is smaller with the increase of the Y atomic mass, consistent with the shortening of the Si···X distance. However, the larger ratio is found for the Si···X interaction with the same Y atom when the X atomic mass is increased. This indicates that the Si···X interaction with the different X and the same Y is weaker for the heavier X atom.

Upon the formation of Si···X interaction, the X−Y bond is elongated in all complexes. Furthermore, its elongation is increased in the order of Y = F < Cl < Br < I when X is hold but is decreased in the order of X = P > As > Sb in most complexes except the **1**···XH_2F complex. In **1**···XH_2F, the elongation of X−Y bond is irregular with the variation of X atom.

Accompanied with the elongation of X−Y bond, the bond stretch vibration displays a red shift. The magnitude of the X−Y stretch shift is consistent with the amount of the X−Y bond elongation in some cases, while such consistence is not found in other cases. The main reason is that the X−Y stretch vibration is involved with the different X and Y atoms in all complexes. The elongation of X−Y bond and the respective red shift are mainly attributed to the charge transfer from the lone pair on the Si atom to the antibonding orbital of X−Y bond.

3.2. Interaction energies

Interaction energies were calculated with supermolecular method and corrected for BSSE and deformation energy (DE). When the interaction energy is corrected for

only BSSE, it is represented as ΔE_1. When both BSSE and DE corrections are considered in the interaction energy, it is expressed as ΔE_2. The values of ΔE_1 and ΔE_2 are collected in Table 3. Obviously, ΔE_2 is more negative than ΔE_1, and their difference grows up in the order of F < Cl < Br < I but is decreased in the order of P > As > Sb. Consequently, the largest difference is -44.1 kJ/mol in **1**···PH_2I, while the smallest one is -10.8 kJ/mol in **1**···SbH_2F. Clearly, the influence of DE on the interaction energy is so prominent that it is necessary to correct the interaction energy with BSSE and DE simultaneously.

Fig. 5 shows the relationship of the interaction energy with the Si···X distance. A good linear relationship is present between the interaction energy and the Si···X distance in the P complexes. Such correlation is also found in the As and Sb complexes except **1**···AsH_2I and **1**···SbH_2I. The Si···X interactions exhibit relatively high interaction energies of -59.9 ~ -105.4 kJ/mol and considerably lengthened X–Y distances with the most value of 0.285 Å. These results are similar to those in halogen bonds between F–Cl and CN–R molecules.[56] Politzer and Murray ascribed these anomalous features to the strong polarization of the CN–R carbon by the electric field of the positive σ-hole of the F–Cl chlorine, resulting in some degree of dative sharing of electrons by the carbons.[56]

In general, the interaction energy of the same Si···X interaction becomes more negative in the order of F < Cl < Br < I. This order was also observed in pnicogen-bonded complexes involving radicals.[33] With the increase of the Y atomic number, the increasing sequence of the interaction energy is reverse to the most

positive MEP on the X atom, which becomes smaller (Table 2). The greater electronegativity of the halogen atom results in the more positive MEP on the X atom. Unfortunately, the related explanation for this contradiction was not given in the previous studies.[33] We should keep in mind that the good relation between the electrostatic potentials and interaction strengths that are followed for noncovalent interactions may not be observed for the strengths of covalent interactions. Based on the above results, we think that the electrostatic interaction is not a sole decisive factor for stabilizing the Si···X interaction.

In the discussion of the geometries, we have successfully applied both types of orbital interactions to explain the structural difference between the different X complexes. Thus we try to unify the contradiction between the interaction energy and the more positive MEP on the X atom by means of both orbital interactions. Unluckily, the second-order perturbation energies due to both types of orbital interactions are not found for these complexes in the NBO calculations due to the formation of Si-X bond. However, it is known that these orbital interactions may lead to the changes of the occupancies in the corresponding orbitals. So the changes of the occupancies in the corresponding orbitals of $LP_{Si}\rightarrow BD^*_{X\text{-}Y}$ and $LP_X\rightarrow LP^*_{Si}$ orbital interactions in the complexes are given in Table 4. It is expected that the occupancies in LP_{Si} and LP_X orbitals are decreased due to their nature of the electron donor orbitals in the orbital interactions, while those in $BD^*_{X\text{-}Y}$ and LP^*_{Si} orbitals are increased because of their nature of the electron acceptor orbitals in the orbital interactions. Moreover, the stronger orbital interactions result in the more changes of the occupancies in the

orbitals. It is found that the changes of the occupancies in LP_{Si} and BD^*_{X-Y} orbitals are much larger than those in LP_X and LP^*_{Si} orbitals. Thus the $LP_{Si}\rightarrow BD^*_{X-Y}$ orbital interaction is stronger than the $LP_X\rightarrow LP^*_{Si}$ one in the Si···X interaction. With the increase of the Y atomic mass in the same Si···X interaction, the occupancies in these orbitals all have an increase in magnitude. Such change is consistent with the increase of the interaction energy of the same Si···X interaction, indicating that the orbital interactions play an important role in the formation of the Si···X interaction.

On the other hand, the interaction energy of the different Si···X interaction is less negative in the order of P > As > Sb for the same halogen substitution except the F one. Similarly, this order is also reverse to the change of the most positive MEP on the X atom, exhibiting the increasing tendency with the same order. However, the occupancies in the orbitals of both $LP_{Si}\rightarrow BD^*_{X-Y}$ and $LP_X\rightarrow LP^*_{Si}$ orbital interactions are decreased with the increase of the X atomic mass. It is also found from Table 4 that the changes of the occupancies in the LP_{Si} and BD^*_{X-Y} orbitals of the $LP_{Si}\rightarrow BD^*_{X-Y}$ orbital interaction have a larger dependence on the Y atom than on the X atom. Of course, the electrostatic contribution is also very important. This can be supported by the results of energy decomposition in Table 5. The interaction energy is decomposed into three terms of electrostatic energy (ES), Pauli repulsion (PR), and orbital interaction (OI). Obviously, the ES contribution is larger than OI one. Of course, both terms are comparable in most complexes, particularly in **1**···PH_2Y. Furthermore, the ratio of OI/ES is increased with the increase of the Y atomic mass but is decreased with the increase of the X atomic mass. The former is consistent with

the change of the occupancy, while the latter is inconsistent with the change of the occupancy. Importantly, the decrease of this ratio with the increase of the X atomic mass is more prominent than its increase with the increase of the Y atomic mass. That is, the electrostatic interaction has major responsibility for the enhancement of Si···X interaction for the larger X complex.

3.3 AIM and charge transfer analyses

The existence of the X···Si interaction in **1**···XH_2Y and the H···H interaction in **1**···SbH_2Y can be characterized with the presence of X···Si and H···H bond critical points (BCPs) in Fig. 6. Simultaneously, a ring critical point is found in **1**···SbH_2Y, corresponding to the cyclic structure. The electron density (ρ), Laplacian ($\nabla^2\rho$), and energy density (*H*) at the respective BCPs are given in Table 6. The electron density at the same Si···X BCP increases as the halogen substituent varies from F to I, with the same trend to the change of the interaction energy. It was acknowledged that the sign of $\nabla^2\rho$ and *H* is a useful indicator of interaction types.[57] The negative $\nabla^2\rho$ and *H* at the Si···P and Si···As BCPs show that the Si···P and Si···As interactions are covalent in nature, whereas the positive $\nabla^2\rho$ and negative *H* at the Si···Sb BCP indicate the partially covalent character of Si···Sb interaction in the Sb complexes. Grabowski presented a review on the covalency of hydrogen bonding and discussed it mainly based on the topological parameters.[58] Clearly, his statements on hydrogen bonding are in force for the Si···X interactions. The positive $\nabla^2\rho$ and *H* at the H···H BCP correspond to a weak interaction mainly driven by electrostatic interaction with the small electron density. Furthermore, the H···H interaction in **1**···SbH_2Y is independent

of the nature of the Y atom because the electron density at the H···H BCP is almost equal in the different **1**···SbH_2Y.

The analyses of orbital interactions and AIM indicate the nature of covalent or partially covalent interaction for the Si···X pnicogen bond. This feature is accompanied with the large charge transfer, which can be estimated with the sum of charge on all atoms of XH_2Y (q_{XH2Y}). The total charge of XH_2Y in the monomer is 0, so q_{XH2Y} in the complex can be treated as the net charge transfer between the two molecules. One can see from Table 4 that the amount of q_{XH2Y} is negative, confirming the role of the electron acceptor for XH_2Y in the Si···X pnicogen bond. This charge transfer increases successively as the Y atom varies in the sequence of F → Cl → Br → I, also supporting the change of the interaction energy. Comparing with the different pnicogen donor, the amount of q_{XH2Y} is reduced for the heavier X atom in the **1**···XH_2Y (Y = Cl, Br, and I) complexes except **1**···XH_2F. We also focus on the change of charge (Δq_{Si}) on the Si atom in the complexes. The magnitude of Δq_{Si} is positive, confirming the conclusion that the LP_{Si}→$BD^*_{X\text{-}Y}$ orbital interaction is stronger than the LP_X→LP^*_{Si} one. Generally, the change of Δq_{Si} is similar to that of q_{XH2Y}.

Both LP_{Si}→$BD^*_{X\text{-}Y}$ and LP_X→LP^*_{Si} orbital interactions cause an electronic rearrangement that occurs upon the formation of each complex, but there are also internal rearrangements within each monomer. The electron density shifts in **1**···PH_2Cl, **1**···AsH_2Cl, and **1**···SbH_2Cl are shown in Fig. 7, where red regions represent charge buildup and depletion of density is indicated by blue. These maps were generated by comparing the electron density in the complex with the sum of the electron densities

of the isolated subsystems frozen in the optimized structure of the complex. There is a similar pattern in all of these dimers. A red increase occurs on the lone pair of the Si atom, in concert with a larger area of charge loss immediately to the σ-hole of X atom. Both changes are like those in conventional pnicogen bonds.[19] A similar charge loss simultaneously is observed on the unoccupied *p* orbital on the Si atom. There is a general reduction of the magnitudes as X varies from P to Sb.

4. Conclusions

Pnicogen-bonded complexes **1**···XH_2Y (**1** = $(H_3P{=}N)_2Si$; X = P, As, and Sb; Y = F, Cl, Br, and I) have been investigated at the MP2/aug-cc-pVTZ level. The results showed that singlet silylene $(H_3P{=}N)_2Si$ can act as the electron donor to interact with the σ-hole of XH_2Y. The H···H interaction was also found in **1**···SbH_2Y and it made this complex losing C_s symmetry. The structure of **1**···XH_2Y was controlled mainly by two orbital interactions of $LP_{Si}\rightarrow BD^*_{X\text{-}Y}$ and $LP_X\rightarrow LP^*_{Si}$. The Si···X interaction is very strong with the big interaction energy ranging from -59.9 to -105.4 kJ/mol and exhibits a nature of covalent or partially covalent bond, confirmed by the negative energy density and the great charge transfer. The energy decomposition indicated that the orbital interaction is comparable with the electrostatic interaction. The strength of Si···X interaction becomes greater for the larger Y atom but is weaker for the larger X atom, showing the reverse change with the MEP of σ-hole on the X atom. This contradiction has been explained with the change of the occupancies in the orbitals of $LP_{Si}\rightarrow BD^*_{X\text{-}Y}$ and $LP_X\rightarrow LP^*_{Si}$ orbital interactions and the amount of charge transfer. Based on the big strength and the great red shift of X-Y stretch vibration in the Si···X

interaction as well as the stability of $(H_3P{=}N)_2Si$, our study may motivate experimentalists to search for the title complexes by spectroscopic methods.

Acknowledgements

This work was supported by the Outstanding Youth Natural Science Foundation of Shandong Province (JQ201006) and the Program for New Century Excellent Talents in University (NCET-2010-0923).

References

1 S. Zahn, R. Frank, E. Hey-Hawkins and B. Kirchner, *Chem. −Eur. J.,* 2011, **17**, 6034−6038.

2 G. Sánchez-Sanz, C. Trujillo, I. Alkorta and J. Elguero, *Phys. Chem. Chem. Phys.,* 2014, **16**, 15900−15909.

3 L. Y. Guan and Y. R. Mo, *J. Phys. Chem. A,* 2014, **118**, 8911−8921.

4 M. Solimannejad and A. Gholipour, *Struct. Chem*., 2012, **24**, 1705−1711.

5 U. Adhikari and S. Scheiner, *Chem. Phys. Lett.,* 2012, **532**, 31−35.

6 J. E. Del Bene, I. Alkorta, G. Sánchez-Sanz and J. Elguero, *J. Phys. Chem. A,* 2012, **116**, 3056−3060.

7 J. E. Del Bene, I. Alkorta, G. Sánchez-Sanz and J. Elguero, *J. Phys. Chem. A,* 2012, **116**, 13724−13731.

8 J. E. Del Bene, I. Alkorta, G. Sánchez-Sanz and J. Elguero, *Chem. Phys. Lett.,* 2011, **512**, 184−187.

9 A. Sánchez-González, S. Melchor, J. A. Dobado, B. Silvi and J. Andrés. *J. Phys. Chem. A,* 2011, **115**, 8316−8326.

10 S. Scheiner, *Phys. Chem. Chem. Phys.,* 2011, **13**, 13860−13872.

11 M. Solimannejad, M. Gharabaghi and S. Scheiner, *J. Chem. Phys*., 2011, **134**, 024312

12 S. Scheiner, *J. Chem. Phys*., 2011, **134**, 164313

13 S. Scheiner, *J. Chem. Phys*., 2011, **134**, 094315

14 S. Scheiner, *Acc. Chem. Res*., 2013, **46**, 280−288.

15 I. Alkorta, G. Sánchez-Sanz, J. Elguero and J. E. Del Bene, *J. Phys. Chem. A,* 2013, **117**, 183−191.

16 S. Scheiner, *CrystEngComm,* 2013, **15**, 3119−3124.

17 P. Politzer, J. S. Murray and T. Clark, *Phys. Chem. Chem. Phys.*, 2013, **15**, 11178−11189.

18 P. Politzer, J. S. Murray, G. V. Janjić and S. D. Zarić, *Crystals*, 2014, **4**, 12−31.

19 S. Scheiner, *J. Phys. Chem. A,* 2011, **115**, 11202−11209.

20 S. Scheiner, *Chem. Phys*., 2011, **387**, 79−84.

21 E. S. Kryachko and T. Zeegers-Huyskens, *J. Phys. Chem. A,* 2002, **106**, 6832−6838.

22 J. S. Murray, P. Lane and P. Politzer, *Int. J. Quantum Chem*., 2007, **107**, 2286–2292.

23 P. Politzer, J. S. Murray and M. C. Concha, *J. Mol. Model.*, 2008, **14**, 659–665.

24 P. Politzer, J.S. Murray and T. Clark, *Phys. Chem. Chem. Phys.*, 2010, **12**, 7748–7757.

25 X. L. An, R. Li, Q. Z. Li, X. F. Liu, W. Z. Li and J. B. Cheng, *J. Mol. Model.,* 2012, **18***,* 4325−4332.

26 G. Sánchez-Sanz, C. Trujillo, M. Solimannejad, I. Alkorta and J. Elguero, *Phys. Chem. Chem. Phys.,* 2013, **15**, 14310−14318.

27 I. Alkorta, J. Elguero and J. E. Del Bene. *J. Phys. Chem. A,* 2013, **117**, 10497−10503.

28 S. Scheiner and U. Adhikari, *J. Phys. Chem. A,* 2011, **115**, 11101−11110.

29 A. Bauzá, D. Quiñonero, P. M. Deyà and A. Frontera. *Phys. Chem. Chem. Phys.*, 2012, **14**, 14061−14066.

30 A. Bauzá, D. Quiñonero, P. M. Deyà and A. Frontera. *CrystEngComm,* 2013, **15**, 3137−3144.

31 H. Y. Xu, W. Wang and J. W. Zou. *Acta Chim. Sinica,* 2013, **71**, 1175−1182.

32 Q. Z. Li, R. Li, X. F. Liu, W. Z. Li and J. B. Cheng, *J. Phys. Chem. A,* 2012, **116**, 2547−2553.

33 I. Alkorta, J. Elguero and M. Solimannejad, *J. Phys. Chem. A,* 2014, **118**, 947−953.

34 J. E. Del Bene, I. Alkorta and J. Elguero, *J. Phys. Chem. A,* 2014, **118**, 3386−3392.

35 I. Alkorta, I. Rozas and J. Elguero, *Chem. Soc. Rev.,* 1998, **27**, 163−170.

36 I. Alkorta and J. Elguero, *J. Phys. Chem*., 1996, **100**, 19367−19370.

37 Q. Z. Li, Y. L. Wang, Z. B. Liu, W. Z. Li, J. B. Cheng, B. A. Gong and J. Z. Sun, *Chem. Phys. Lett.,* 2009, **469**, 48−51.

38 M. D. Esrafili, F. Mohammdain-Sabet and P. Esmailpour, *J. Mol. Model*., 2013, **19**, 4797−4804.

39 M. D. Esrafili and F. Mohammdain-Sabet, *J. Mol. Model*., 2013, **19***,* 2559−2566.

40 Q. Z. Li, H. Z. Wang, Z. B. Liu, W. Z. Li, J. B. Cheng, B. A. Gong and J. Z. Sun, *J. Phys. Chem. A,* 2009, **113**, 14156−14160.

41 Q. Zhao, D. C. Feng, Y. M. Sun, J. C. Hao and Z. T. Cai, *Int. J. Quantum. Chem.* 2011, **111**, 3881−3887.

42 A. K. Biswas, R. Lo and B. Ganguly, *J. Phys. Chem. A,* 2013, **117**, 3109−3117.

43 S. F. Boys and F. Bernardi, *Mol. Phys.,* 1970, **19**, 553−566.

44 M. J. Frisch, G. W. Trucks, H. B. Schlegel, G. E. Scuseria, M. A. Robb, J. R. Cheeseman, G. Scalmani, V. Barone, B. Mennucci, G. A. Petersson, H. Nakatsuji, M. Caricato, X. Li, H. P. Hratchian, A. F. Izmaylov, J. Bloino, G. Zheng, J. L. Sonnenberg, M. Hada, M. Ehara, K. Toyota, R. Fukuda, J. Hasegawa, M. Ishida, T. Nakajima, Y. Honda, O. Kitao, H. Nakai, T. Vreven, J. J. A. Montgomery, J. E. Peralta, F. Ogliaro, M. Bearpark, J. J. Heyd, E. Brothers, K. N. Kudin, V. N. Staroverov, R. Kobayashi, J. Normand, K. Raghavachari, A. Rendell, J. C. Burant, S. S. Iyengar, J. Tomasi, M. Cossi, N. Rega, J. M. Millam, M. Klene, J. E. Knox, J. B. Cross, V. Bakken, C. Adamo, J. Jaramillo, R. Gomperts, R. E. Stratmann, O. A. Yazyev, J. Austin, R. Cammi, C. Pomelli, J. W. Ochterski, R. L. Martin, K. Morokuma, V. G. Zakrzewski, G. A. Voth, P. Salvador, J. J. Dannenberg, S. A. Dapprich, D. Daniels, O. Farkas, J. B. Foresman, J. V. Ortiz, J. Cioslowski and D. J. Fox, *Gaussian 09,* Revision A.02. Gaussian, Inc.: Wallingford CT, 2009.

45 F. A. Bulat, A. Toro-Labbé, T. Brinck, J. S. Murray and P. Politzer, *J. Mol. Model.*, 2010, **16**, 1679−1691.

46 A. E. Reed, L. A. Curtiss and F. Weinhold, *Chem. Rev.*, 1988, **88**, 899−926.

47 R. F. W. Bader, AIM2000 Program, v 2.0; McMaster University, Hamilton, Canada, 2000.

48 T. Lu and F. W. Chen, *J. Comput. Chem.,* 2012, **33**, 580−592.

49 ADF2008.01 SCM, Theoretical Chemitry, Vrije Universieit, Amsterdam, The Netherlands, http://www.scm.com.

50 J. S. Murray and P. Politzer, *WIREs Comput. Mol. Sci.,* 2011, **1**, 153−163.

51 I. Alkorta, J. Elguero and J. E. Del Bene. *J. Phys. Chem. A,* 2013, **117**, 4981−4987.

52 J. E. Del Bene, I. Alkorta, G. Sánchez-Sanz and J. Elguero, *J. Phys. Chem. A,* 2013, **117**, 3133−3141.

53 U. Adhikari and S. Scheiner, *J. Chem. Phys.,* 2011, **135**, 184306.

54 N. L. Allinger, X. Zhou, and J. Bergsma, *J. Mol. Struct., Theochem.,* 1994, **312**, 69−83.

55 J. P. M. Lommerse, A. J. Stone, R. Taylor and F. H. Allen, *J. Am. Chem. Soc*., 1996, **118**, 3108−3116.

56 P. Politzer and J. S. Murray, *Theor. Chem. Acc.*, 2012, **131**, 1114

57 J. E. Del Bene, I. Alkorta and J. Elguero, *J. Phys. Chem. A,* 2008, **112**, 7925−7929.

58 S.J. Grabowski, *Chem. Rev*. 2011, **111**, 2597–2625.

Table 1 Si···X and H···H distances (R, Å), change of X-Y bond length ($\Delta r_{X\text{-}Y}$, Å), and frequency shift of X-Y stretch vibration ($\Delta \nu_{X\text{-}Y}$, cm^{-1}) in the complexes

	$R_{Si\cdots X}$	λ	$R_{H\cdots H,\,l}$	$R_{H\cdots H,\,r}$	$\Delta r_{X\text{-}Y}$	$\Delta \nu_{X\text{-}Y}$
1···PH_2F	2.439	0.541	2.820	2.820	0.075	-217.6
1···PH_2Cl	2.385	0.529	2.782	2.782	0.229	-273.8
1···PH_2Br	2.365	0.524	2.777	2.777	0.262	-198.0
1···PH_2I	2.356	0.522	2.793	2.793	0.285	-194.3
1···AsH_2F	2.661	0.572	2.704	2.703	0.089	-165.9
1···AsH_2Cl	2.561	0.551	2.679	2.689	0.225	-143.1
1···AsH_2Br	2.533	0.545	2.676	2.672	0.250	-137.8
1···AsH_2I	2.516	0.541	2.670	2.691	0.265	-112.4
1···SbH_2F	2.902	0.603	2.430	3.036	0.074	-112.1
1···SbH_2Cl	2.863	0.595	2.468	2.918	0.154	-107.3
1···SbH_2Br	2.843	0.591	2.465	2.904	0.177	-87.6
1···SbH_2I	2.827	0.588	2.464	2.916	0.199	-70.2

Note: $R_{H\cdots H,\,l}$ and $R_{H\cdots H,\,r}$ are the distances between the H atom of PH_3 in **1** and the H atom of XH_2Y in the left and right of Fig. 2, respectively. $\lambda = R_{Si\cdots X}/(r_{Si}+r_X)$, where r_{Si} and r_X are the van der Waals radii of Si and X atoms, respectively.

Table 2 Most positive (V_{max}, au) and negative (V_{min}, au) MEPs on the X atom of XH_2Y

	V_{max}	V_{min}
PH_2F	0.0604	-0.0190
PH_2Cl	0.0524	-0.0147
PH_2Br	0.0487	-0.0137
PH_2I	0.0417	-0.0130
AsH_2F	0.0685	-0.0088
AsH_2Cl	0.0585	-0.0068
AsH_2Br	0.0544	-0.0062
AsH_2I	0.0467	-0.0062
SbH_2F	0.0782	0.0016
SbH_2Cl	0.0693	0.0026
SbH_2Br	0.0651	0.0028
SbH_2I	0.0579	0.0027

Table 3 Interaction energies corrected for BSSE (ΔE, kJ/mol) in the complexes

	ΔE_1	ΔE_2
1···PH_2F	-46.4	-59.9
1···PH_2Cl	-52.3	-92.4
1···PH_2Br	-58.2	-102.3
1···PH_2I	-61.3	-105.4
1···AsH_2F	-48.8	-60.9
1···AsH_2Cl	-52.9	-87.3
1···AsH_2Br	-56.1	-93.3
1···AsH_2I	-56.5	-92.5
1···SbH_2F	-59.8	-70.6
1···SbH_2Cl	-59.4	-78.8
1···SbH_2Br	-59.8	-81.2
1···SbH_2I	-58.2	-80.4

Note: Interaction energy is calculated with the formulas of $\Delta E = E_{complex} - (E_{\mathbf{1}} + E_{XH2Y})$, in which $E_{complex}$ is the energy of optimized **1**···XH_2Y complex corrected for BSSE, $E_{\mathbf{1}}$ and E_{XH2Y} are the energies of the corresponding optimized monomers for ΔE_1, while $E_{\mathbf{1}}$ and E_{XH2Y} are the energies of the monomers with the geometries in the complexes for ΔE_2.

Table 4 Sum of charge on all atoms of XH_2Y (q_{XH2Y}, e), change of charge on the Si atom (Δq_{Si}, e), and the change of occupancy (Δn, e) in the corresponding orbitals of $LP_{Si}\rightarrow BD^*_{X\text{-}Y}$ and $LP_X\rightarrow LP^*_{Si}$ orbital interactions in the complexes

	q_{XH2Y}	Δq_{Si}	Δn (LP_{Si})	Δn($BD^*_{X\text{-}Y}$)	Δn(LP_X)	Δn(LP^*_{Si})
1···PH_2F	-0.304	0.258	-0.510	0.397	-0.233	0.117
1···PH_2Cl	-0.486	0.398	-0.667	0.641	-0.283	0.117
1···PH_2Br	-0.534	0.431	-0.712	0.736	-0.320	0.123
1···PH_2I	-0.557	0.444	-0.736	0.830	-0.372	0.131
1···AsH_2F	-0.320	0.257	-0.471	0.318	-0.064	0.075
1···AsH_2Cl	-0.468	0.372	-0.610	0.472	-0.069	0.089
1···AsH_2Br	-0.504	0.397	-0.646	0.518	-0.075	0.097
1···AsH_2I	-0.516	0.402	-0.662	0.552	-0.082	0.108
1···SbH_2F	-0.320	0.236	-0.440	0.288	-0.030	0.055
1···SbH_2Cl	-0.386	0.287	-0.501	0.358	-0.030	0.061
1···SbH_2Br	-0.412	0.309	-0.526	0.370	-0.032	0.065
1···SbH_2I	-0.431	0.321	-0.545	0.415	-0.036	0.071

Table 5 Electrostatic (ES), Pauli repulsion (PR), and orbital interaction (OI) energies as well as the interaction energy (E_{int}) in the complexes at the GGA: BLYP/TZP level. All are in kJ/mol

	ES	PR	OI	OI/ES	E_{int}
1···PH_2F	-302.1	534.1	-270.0	0.89	-38.0
1···PH_2Cl	-356.5	628.3	-318.5	0.89	-46.7
1···PH_2Br	-379.0	667.0	-354.1	0.93	-66.1
1···PH_2I	-388.8	684.3	-363.1	0.93	-67.6
1···AsH_2F	-245.0	391.9	-181.7	0.74	-34.8
1···AsH_2Cl	-316.4	511.7	-246.3	0.78	-51.0
1···AsH_2Br	-338.7	550.3	-266.4	0.79	-54.8
1···AsH_2I	-343.2	562.1	-271.7	0.79	-52.8
1···SbH_2F	-233.4	343.3	-143.8	0.62	-33.9
1···SbH_2Cl	-257.3	381.4	-163.0	0.63	-38.9
1···SbH_2Br	-270.6	403.6	-173.2	0.64	-40.2
1···SbH_2I	-279.1	420.8	-181.7	0.65	-40.0

Table 6 Electron density (ρ, au), Laplacian ($\nabla^2\rho$, au), energy density (*H,* au), kinetic energy density (*G*, au), and potential energy density (*V,* au) at the X···Si BCP in the complexes

	ρ	$\nabla^2\rho$	*G*	*V*	*H*
1···PH_2F	0.0732	-0.0554	0.0169	-0.0477	-0.0308
1···PH_2Cl	0.0811	-0.0814	0.0170	-0.0544	-0.0374
1···PH_2Br	0.0835	-0.0919	0.0171	-0.0572	-0.0401
1···PH_2I	0.0840	-0.0993	0.0172	-0.0592	-0.0420
1···AsH_2F	0.0537	-0.0026	0.0161	-0.0329	-0.0168
1···AsH_2Cl	0.0646	-0.0264	0.0170	-0.0405	-0.0236
1···AsH_2Br	0.0676	-0.0351	0.0170	-0.0427	-0.0257
1···AsH_2I	0.0692	-0.0426	0.0165	-0.0436	-0.0271
1···SbH_2F	0.0418 (0.0063)	0.0181 (0.0163)	0.0152 (0.0035)	-0.0259 (-0.0030)	-0.0107 (0.0006)
1···SbH_2Cl	0.0452 (0.0059)	0.0131 (0.0156)	0.0156 (0.0033)	-0.0281 (-0.0028)	-0.0124 (0.0006)
1···SbH_2Br	0.0470 (0.0060)	0.0102 (0.0157)	0.0159 (0.0034)	-0.0292 (-0.0028)	-0.0133 (0.0006)
1···SbH_2I	0.0485 (0.0060)	0.0063 (0.0157)	0.0157 (0.0034)	-0.0298 (-0.0028)	-0.0141 (0.0006)

Note: Data in parentheses are from the H···H BCP in Fig. 6.

Figure captions

Fig. 1 MEP and ELF maps of the monomers. Color ranges for MEPs (in au) are: red, greater than 0.03; yellow, between 0.03 and 0.00; green, between 0.00 and -0.01; blue, less than -0.01. Isosurface =

0.85 au for ELF.

Fig. 2 Optimized structures of **1**···XH_2Y (X = P, As, Sb; Y = F, Cl, Br, I).

Fig. 3 Side view of **1**···PH_2Y, **1**···AsH_2Y, and **1**···SbH_2Y (Y = F, Cl, Br, I).

Fig. 4 Orbital interactions between **1** and XH_2Y.

Fig. 5. Relationship of the interaction energy and the Si···X distance in **1**···XH_2Y.

Fig. 6 Molecular graphs of **1**···XH_2Y (X = P, As, and Sb; Y = F, Cl, Br, and I). Small red pointes are BCPs and yellow one is RCP.

Fig. 7 Electron density difference maps of **1**···PH_2Cl, **1**···AsH_2Cl, and **1**···SbH_2Cl. Red regions represent the increase of electron density and blue regions represent the decrease of electron density. Contours are shown at the 0.002 au level.

Fig. 1

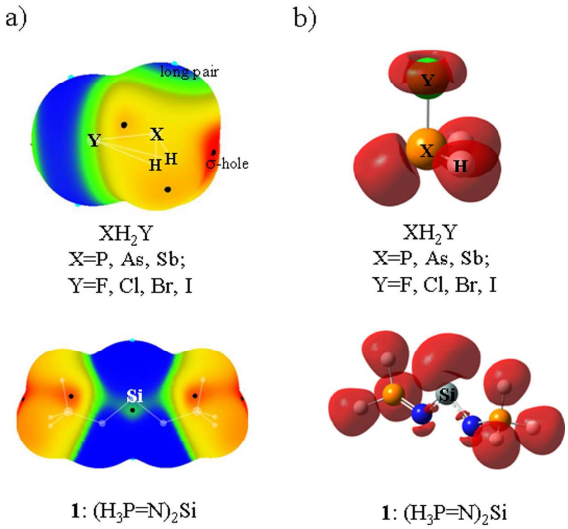

Fig. 2

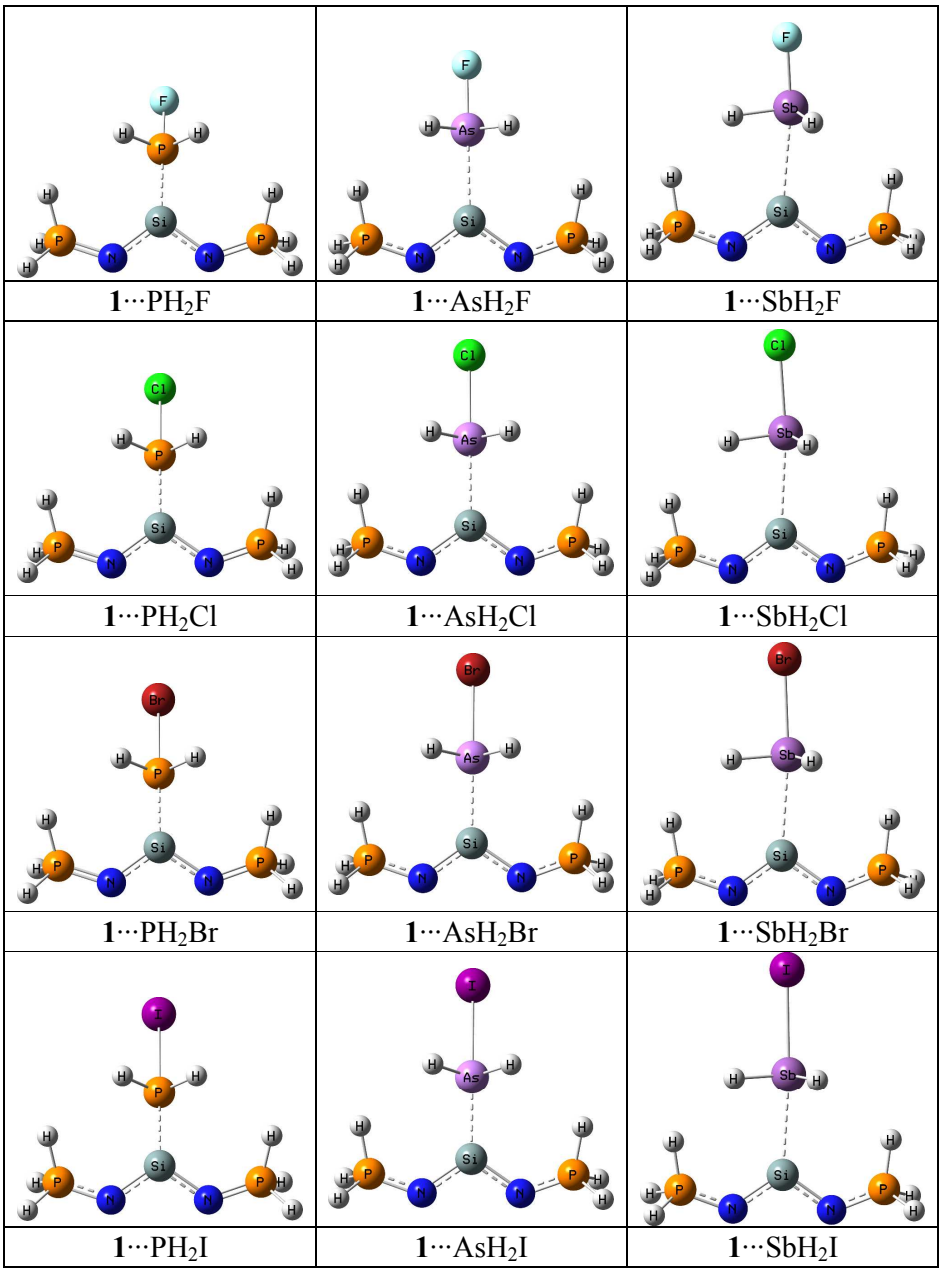

Fig. 3

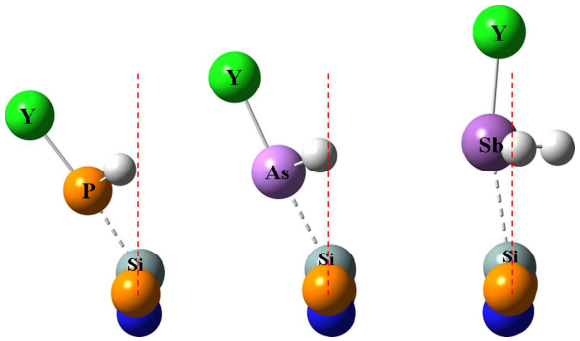

Fig. 4

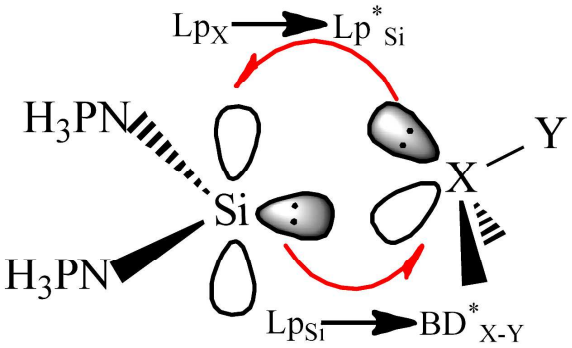

Fig. 5

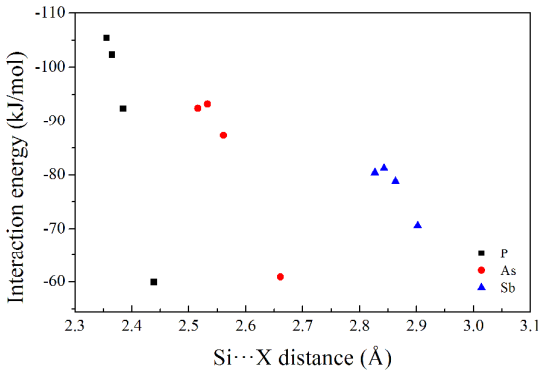

Fig. 6

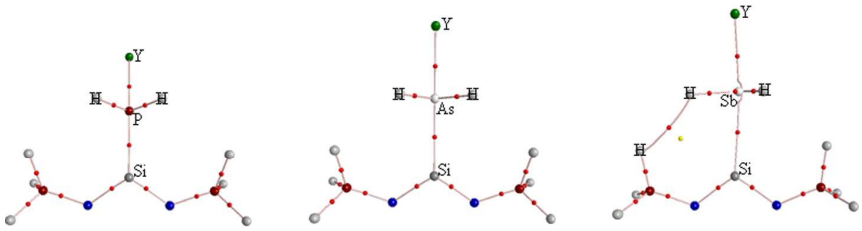

1···PH_2Y (Y=F, Cl, Br, I) **1**···AsH_2Y (Y=F, Cl, Br, I) **1**···SbH_2Y (Y=F, Cl, Br, I)

Fig. 7

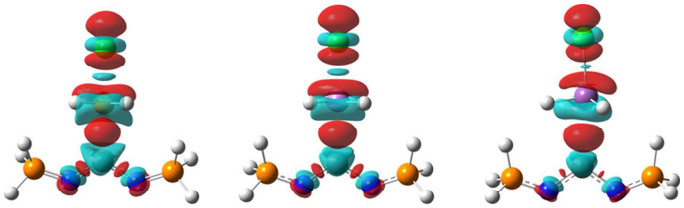

1···PH_2Cl **1**···AsH_2Cl **1**···SbH_2Cl

TOC

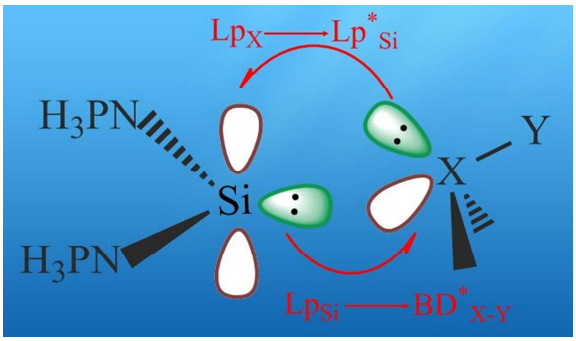

A new pnicogen bonding involving silylene was proposed and characterized, exhibiting unexpected substituent effect and dependence on the pnicogen atom.